THE INTERNATIONAL JOURNAL OF SCIENCE & TECHNOLEDGE

Hydrometallurgical Processing of a Nigerian Sphalerite Ore in Nitric Acid: Characterization and Dissolution Kinetics

Okechukwu D. Onukwuli
Professor of Chemical Engineering, Nnamdi Azikiwe University, Nigeria
Ikechukwu A. Nnanwube
Ph.D. Student, Department of Chemical Engineering, Nnamdi Azikiwe University, Nigeria

Abstract:
The results of experimental investigation on the dissolution kinetics of a Nigerian sphalerite ore in nitric acid solution were discussed. The effects of acid concentration, temperature, particle size, stirring speed and soild/liquid ratio on the leaching of sphalerite was examined. The results of the elemental analysis of sphalerite by X-ray fluorescence (XRF) showed that the sphalerite mineral exist mainly as ZnS with metals such as Fe, Na, Mg, Al, Ca, Mn, P, Ti, and Cr occurring as minor or trace elements. The XRD result confirmed the originality of the sphalerite sample as it revealed the presence of sphalerite (ZnS) as the dominant mineral and cerium germanium sulphide (Ce_2GeS_2) as an associated mineral. The scanning electron micrograph (SEM) result revealed a high level of crystallinity of the sample, indicating a high level of purity. The FTIR analysis also confirmed the presence of sulphur in the sphalerite ore. The leaching experiments showed that sphalerite dissolution in nitric acid increases with increase in acid concentration, temperature and stirring speed and decreases with increase in solid/liquid ratio and particle diameter. In 10M HNO_3 at a temperature of 363K using 75µm particle diameter with solid/liquid ratio of 20g/L and stirring speed of 540 rpm, about 86.6% of sphalerite was dissolved. The values of activation energy, reaction order, Arrhenius constant and reaction constant calculated at the conditions above were 26.42KJ/mol, 0.91, 23.06s^{-1} and 5.23 × 10^7 respectively. The kinetic data analysis suggested that the shrinking core model for spherical particles is applicable and thus, the leaching reaction follow the diffusion controlled mechanism, with the surface chemical reaction as the rate determining step. The XRD analysis of the post-leaching residue revealed the presence of sulphur, quartz and sylvite.

Keywords: *Sphalerite, Nigeria, characterization, leaching, dissolution kinetics, nitric acid*

1. Introduction

Sphalerite is the most important ore of zinc. Around 95% of all primary zinc is extracted from sphalerite ores. However, due to its variable trace element content, sphalerite is also an important source of many minor metals, such as cadmium , gallium (Frenzel et al., 2016), germanium (Frenzel et al., 2014), and indium (Frenzel et al., 2017). Crystals of suitable size and transparency have been fashioned into gemstones, usually featuring the brilliant cut to best display sphalerite's high dispersion-over three times that of diamond. A variety of zinc compounds are used industrially. Zinc oxide is widely used as a white pigment in paints, and as a catalyst in the manufacture of rubber. It is also used as a heat disperser for the rubber and acts to protect its polymers from ultraviolet radiation (the same UV protection is conferred to plastics containing zinc oxide) (Emsley, 2001). The semiconductor properties of zinc oxide make it useful in varistors and photocopying products (Zhang, 1996). Zinc sulphide (ZnS) is used in luminescent pigments such as on the hands of clocks, X-ray and television screens, and luminous paints (David, 2006). Crystals of ZnS are used in lasers that operate in the mid-infrared part of the spectrum (Paschotta, 2008). Zinc sulphate is a chemical in dyes and pigments (Heiserman, 1992). Zinc pyrithione is used in antifouling paints (Konstantinou and Albanis, 2004).

1.1. Sphalerite Ore Characterization

Several studies on the characterization of sphalerite ore have been carried out in the recent years. Some of the reported results on the composition of sphalerite from different parts of the world are summarized in Table 1.

Sphalerite is composed of zinc as a dominant metal followed by sulphur and iron in that order. The composition of sphalerite varies from one location to another. The different values can be accounted for by the variation in geochemical and environmental effects. In particular, the difference in the associated minerals, soil type, temperature and other climatic conditions may have great influence on the mineral composition. In all cases, the dominant elements in the sphalerites are zinc and sulphur, withcontent varying between 27 and 39% (Adekola and Baba, 2010).

1.2. Sphalerite Dissolution Kinetic Studies

A number of researchers have carried out some studies on the dissolution of sphalerite in acid and oxidative reagents as detailed below. Sokic et al., (2012) studied the kinetics and mechanism of sphalerite leaching from complex sulphide concentrate with sulphuric acid and sodium nitrate solution at saturated conditions. The results showed that with temperature increasing from 60 to 90^{o}C, the zinc leaching increased from 25.23% to 71.66% after 2 hours and from 59.40% to 99.83% after 4 hours. The selected kinetic model indicated that the diffusion through the product layer was the rate-controlling step during the sphalerite leaching. The activation energy was determined to be 55 KJ/mol in the temperature range of 60-90^{o}C.

Adebayo et al., (2006) investigated the leaching of powdered sphalerite using hydrogen peroxide and nitric acid. The important variables such as concentrations of hydrogen peroxide, nitric acid, stirring speed, particle size as well as the effect of reaction temperature on the leaching process were also examined. The results showed that the hydrogen peroxide and nitric acid concentrations had significant effects on the leaching of sphalerite. The leaching of sphalerite was dependent on temperature and stirring speed and inversely proportional on the ore particle size. The apparent activation energy was found to be 28.7 KJmol^{-1} suggesting that the reaction was chemical-controlled at the surface of the particles.

Majima et al. (1981) carried out a kinetic study on non-oxidative dissolution of sphalerite in hydrochloric acid solutions using sphalerite obtained from Japan. 12 M of HCl was used and the activation energy was obtained as 84.0 KJ/mol.

Aydogan et al. (2005) studied the dissolution kinetics of sphalerite in acidic ferric chloride leaching using sphalerite obtained from Sivas, Turkey. 0.25M $FeCl_3$ was used in the presence of 0.1 M HCl. The activation energy was obtained as 45.3 KJ/mol.

Leao et al., (2007) examined the dissolution kinetics of an iron-rich zinc sulphide concentrate in acid ferric sulphate medium. The effects of temperature, ferric ion and sulphuric acid concentrations, agitation speed and particle size on the leaching kinetics were investigated. The leaching process was separated into two stages. Initially, it was found that the dissolution kinetics was controlled by the chemical reaction at the surface of the zinc sulphide particles followed by a second step where the reaction was controlled by diffusion of the reagents or products through the elemental sulphur (ash) layer. The activation energy of the chemical controlled step was 27.5 KJ/mol and the value determined for the diffusion controlled step was 19.6 KJ/mol. The reaction order with respect to ferric ion and sulphuric acid concentrations were approximately 0.5 and 1.00, respectively. Analysis of the unreacted and reacted sulphide particles by SEM-EdS showed a progressive increase of the thickness of the elemental sulphur layer on the solid surface.

Al-Harahsheh and Kingman (2007) studied the leaching kinetics of pure sphalerite crystals in acidic ferric chloride under conventional and microwave-heated conditions. The effects of stirring speed, particle size, ferric chloride concentration and temperature were investigated. The shrinking core model was applied to the results of the experiments. It was found that the reaction was controlled by chemical reaction with activation energy of 44.8K J/mol. The order of reaction with respect to the ferric chloride concentration was found to be 0.62. The effect of microwaves on the leaching of sphalerite in acidic ferric chloride was also investigated. An enhancement on the zinc recovery was observed which was more apparent at stagnant conditions (rather than stirred) when compared to conventional leaching.

Hydrometallurgical studies, particularly on the chemical leaching of Nigerian sphalerite are very limited. The few major works done so far include those of Olanipekun and Oderinde (Olanipekun and Oderinde, 1999) and Adekola and Baba (Adekola and Baba, 2010). This work is therefore expected to be a good reference material on sphalerite from Nigeria.

Reference	Location	Major elemental composition (%)								
		Zn	Pb	Fe	S	Cu	Ca	Ag	Sb	Mn
Aydogan et al. (2005)	Sivas, Turkey	57.87	NA	0.98	29.32	NA	NA	NA	NA	NA
Madhuchhauda et al. (2000)	Bhubaneswar, India	46.65	2.16	7.49	37.00	0.06	NA	NA	NA	NA
Zuo-mei et al.(1984)	China	61.50	0.11	3.40	NA	0.86	NA	NA	NA	NA
Harvey and Yen (1998)	Gouvenour, Canada	52.20	0.10	4.30	NA	0.05	NA	NA	NA	NA
Peng et al.(2005)	Beijing, China	50.00	3.00	7.00	31.00	0.08	0.02	0.01	0.14	NA
Ballester et al. (1998)	Asturias, Spain	62.80	NA	1.51	30.80	0.09	NA	NA	NA	NA
Pina et al. (2005)	Ouro Preto, Brazil	48.13	NA	12.12	31.02	NA	NA	NA	NA	NA
Sassi and Sassi (1999)	Tunis, Tunisia	43.85	NA	0.03	38.96	NA	NA	NA	NA	4.85
Merwe (2003)	Namibia	32.70	1.19	21.00	27.20	0.67	NA	NA	NA	NA
Adebayo et al.(2006)	Ebonyi, Nigeria	16.40	0.78	7.12	29.20	NA	NA	NA	NA	NA
Goktepe (2002)	Bahkesir, Turkey	66.59	NA	7.84	NA	0.14	NA	NA	NA	NA
Ucar (2009)	Sivas, Turkey	60.14	NA	0.09	30.93	0.05	NA	NA	NA	NA

Table 1: Elemental Composition of Some Sphalerites from Different Parts of the World.
NA: Not Analyzed

2. Materials and Methods

The sphalerite ore used for this study was collected from Abakaliki, Enyigba mining site in Ebonyi State of Nigeria. The ore sample was finely pulverized and sieved into five fractions: 75, 106, 212, 300, and 425 µm. All experiments were performed with 75 µm fraction except otherwise stated. Solutions of HNO_3 were prepared from Analytical grade reagents with deionized water.

2.1. *Characterization of the Ore*

2.1.1. Spectrophotometric Analysis

The X-ray fluorometer (XRF), X-supreme 600 oxford instruments was used for the elemental analysis of the ore. The mineralogical analysis of the ore was done using ARL X'TRA X-ray Diffractometer, Thermoscientific with the serial number 197492086 and Empyrean by PanAnalytical model with CuKα (1.54 Å) radiation generated and 40mA and 45kV. This unit comprises of a single compact cabinet. The cabinet houses a high speed, high precision Goniometer; high efficiency generator (X-ray) and an automatic sample loading facility.

The petrographic slides of sphalerite ore were prepared using Epoxy and Lakeside 70 media according to the method of Hutchison (1974).

2.1.2. FTIR and SEM Analysis

FTIR analysis was carried out using Buck Scientific M530 Infrared Spectrophotometer. SEM analysis was carried out using Q250 by FEI model from the Netherlands.

2.2. Leaching Procedure

Leaching experiments were performed in a 500 ml glass reactor fitted with a condenser to prevent losses through evaporation. The two major variables (heat and stirring rate) necessary for accelerating the rate of chemical reaction was provided by the aid of a magnetically-stirred hot plate (Model 78HW-1). For every leaching experiment, the solution mixture was freshly prepared by dissolving 20 g/L of the ore sample in the acid solution at 363K. The concentration which gave the maximum dissolution was subsequently used to study other leaching parameters including temperature and particle size. At the end of each reaction time, the undissolved materials in the suspension was allowed to settle and separated by filtration. The resulting solutions were diluted and analyzed for the required metal using atomic absorption spectrophotometer (AAS).
The mole fraction of zinc passing into the solution from sphalerite was calculated by the formula given in the equation below, where *x* designates quantity dissolution.

$$x = \frac{\text{Amount of Zn passing into the solution}}{\text{Amount of Zn inoriginal sample}} \quad (1)$$

The activation energy,E_a and rate constants were evaluated from the Arrhenius plots. The post-leached residues after dissolution in the optimum conditions were subjected to XRD and SEM examination.

3. Results and discussion

3.1. Results of Characterization Studies

3.1.1. Elemental Characterization by XRF

The results of the elemental composition of sphalerite by X-ray fluorescence technique showed that the sphalerite mineral exist mainly as ZnS with some quantities of Fe and Na. Metals such as Na, Mg, Al, Ca, and Mn exist as minor elements, while P, Ti, and Cr as traces. The elemental analysis gave Zn (31.67 %), S (29.81 %), Fe (11.97 %), Na (16.32 %), Si (4.66 %), Ca (2.01 %), Al (1.66 %), Mn (1.03 %), Mg (0.61 %), P (0.08 %), Cl (0.14 %), Ti (0.05 %) and Cr (0.01 %).

3.1.2. Phase Studies by XRD

The analysis of sphalerite by X-ray diffraction gives a better description in terms of the mineral phases present in the ore. Table 2 present the results of the X-ray diffractogram of the ore with important compounds identified.
The sphalerite ore gave three major peaks at 3.12, 1.91 and 1.63 Å, respectively as shown in Figure 1. The result also reveals the presence of sphalerite as the dominant mineral and cerium germanium sulphide (Ce_2GeS_2) as an associated mineral. All these supported the results of the elemental analysis by XRF.

2θ	d-Value (Å)	Compound	Intensity (%)	JCPDS file No
26.03	3.42	Cerium Germanium Sulphide (Ce_2GeS_2)	45.95	03-065-8125
28.56	3.12	Sphalerite (ZnS)	100.00	03-065-9585
30.15	2.96	Cerium Germanium Sulphide (Ce_2GeS_2)	100.00	03-065-8125
33.09	2.70	Sphalerite (ZnS)	8.71	03-065-9585
43.16	2.09	Cerium Germanium Sulphide (Ce_2GeS_2)	63.86	03-065-8125

2θ	d-Value (Å)	Compound	Intensity (%)	JCPDS file No
47.50	1.91	Sphalerite (ZnS)	50.45	03-065-9585
51.09	1.79	Cerium Germanium Sulphide (Ce_2GeS_2)	17.62	03-065-8125
53.54	1.71	Cerium Germanium Sulphide (Ce_2GeS_2)	19.72	03-065-8125
56.37	1.63	Sphalerite (ZnS)	26.00	03-065-9585
59.11	1.56	Sphalerite (ZnS)	1.70	03-065-9585

Table 2: The X-Ray Diffraction Data of the Sphalerite Ore Showing the Angle 2θ and D-Values of the Compounds Identified, with Their Relative Intensity (%).
JCPDS File No. : Joint Committee on Power Diffraction Standards File Number

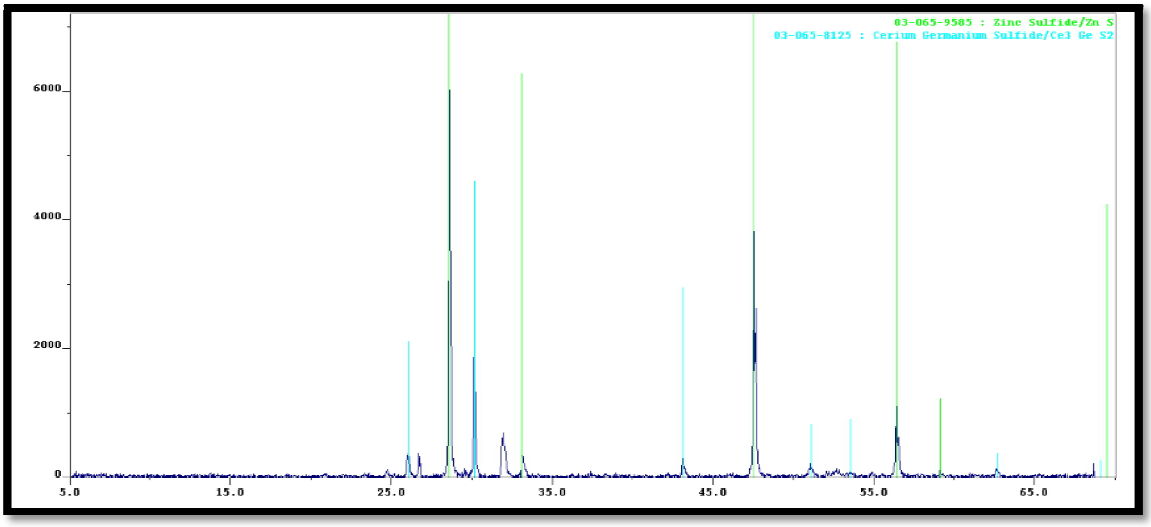

Figure 1: X-Ray Diffraction Pattern of Sphalerite Ore

3.1.3. FTIR Analysis of Sphalerite

The FTIR spectra of sphalerite ore is shown in Figure 2. The spectrum of the ore exhibit absorption bands at 3732 cm^{-1}, 3648 cm^{-1}, 3456 cm^{-1}, 3325 cm^{-1}, 3226 cm^{-1}, 2921 cm^{-1}, 2678 cm^{-1}, 2464 cm^{-1} which are attributed to O-H stretching. The bands at 3456 cm^{-1}, 3325 cm^{-1}, 2678 cm^{-1}, and 2464 cm^{-1} are attributed to N-H stretching. Si-O and Al-O stretching modes associated with tetrahedral polyhedral account for the band at 1036 cm^{-1}. The band at 1320 cm^{-1}, attributed to SO_2 antisymmetric stretch and the band at 745 cm^{-1} attributed to C-S stretch confirm the presence of sulphur in the ore.

The FTIR result is in agreement with XRF and XRD results which confirmed the presence of the minerals detected.

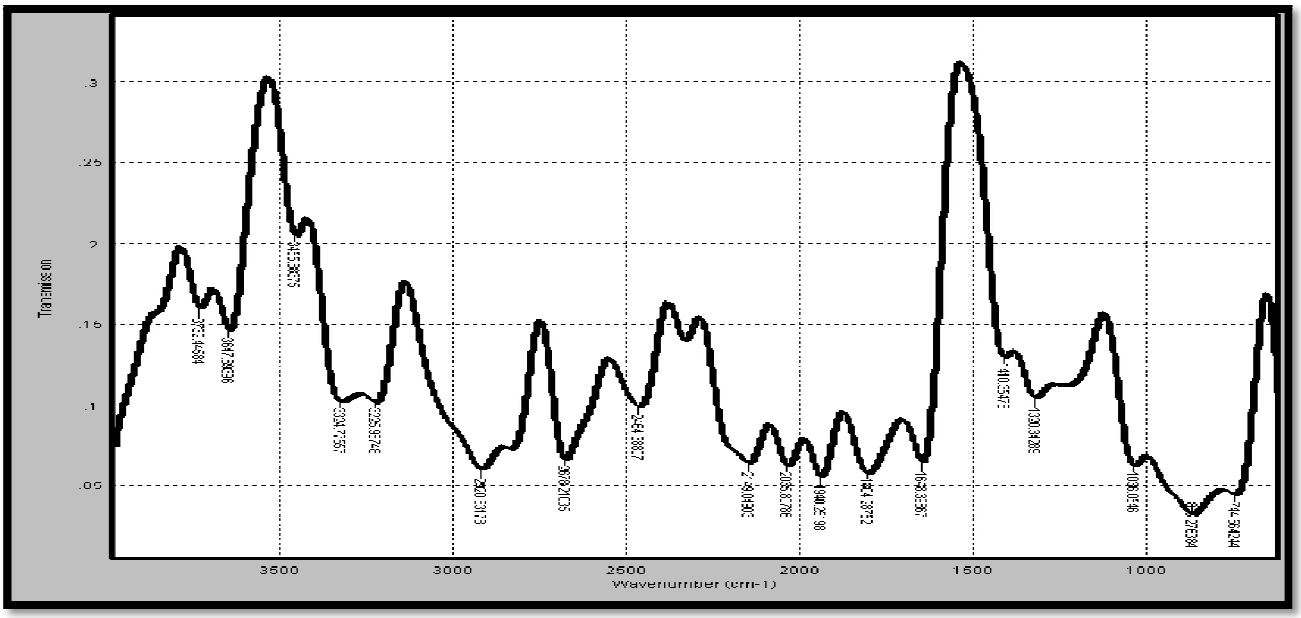

Figure 2: FTIR Spectrum of Sphalerite Ore

3.1.4. SEM Analysis of Sphalerite

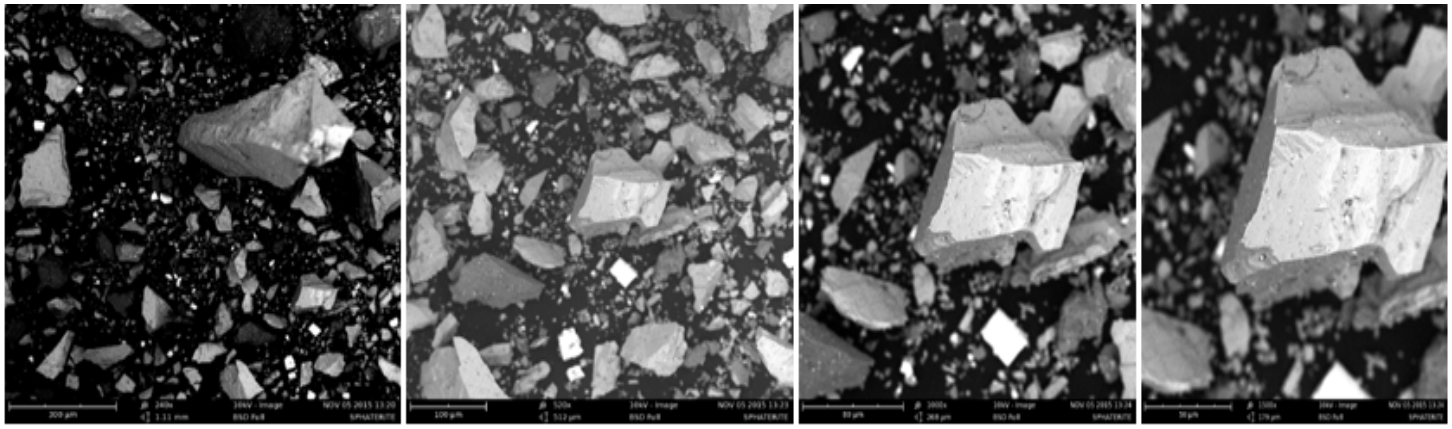

Figure 3: SEM Images of Sphalerite Showing Magnifications of 240× (A), 520× (B), 1000× (C) and 1500× (D) Respectively

The scanning electron micrograph (SEM) of sphalerite ore was obtained with magnifications of 240x, 520x, 1000x and 1500x respectively as shown in Figure 3. The average cell diameter of the ore ranges from 20 to 89 µm while the average cell density ranges from 0.044 to 0.064cell/mm. The results indicate that the particles are very cohesive, confirming their micrometer sized agglomerates with irregular shapes and rough edges and form microscopic flakes (Sthay and Ramaswamy, 2002). The particles are highly crystalline. This is largely due to the high level of purity of the ore.

3.2. Leaching Studies

3.2.1. Effect of HNO_3 Concentration on Sphalerite Dissolution

The results of the effect of HNO_3 concentration on sphalerite dissolution are illustrated in Figure 4. The result shows that the fraction of sphalerite dissolved increases with increasing acid concentration. The results obtained with 12 M HNO_3 is slightly lower than that of 10 M HNO_3, and this could be attributed to a change in the rate determining step due to the significant quantity of elemental sulphur produced (Warren et al., 1986).

In all cases, unreacted acid remained in the leach solution and the free acid increased with increasing initial acid concentration, since the use of more concentrated acid did not increase the dissolution of sphalerite or decrease the leaching time for maximum dissolution. Therefore, 10 M HNO_3 was used for further investigation.

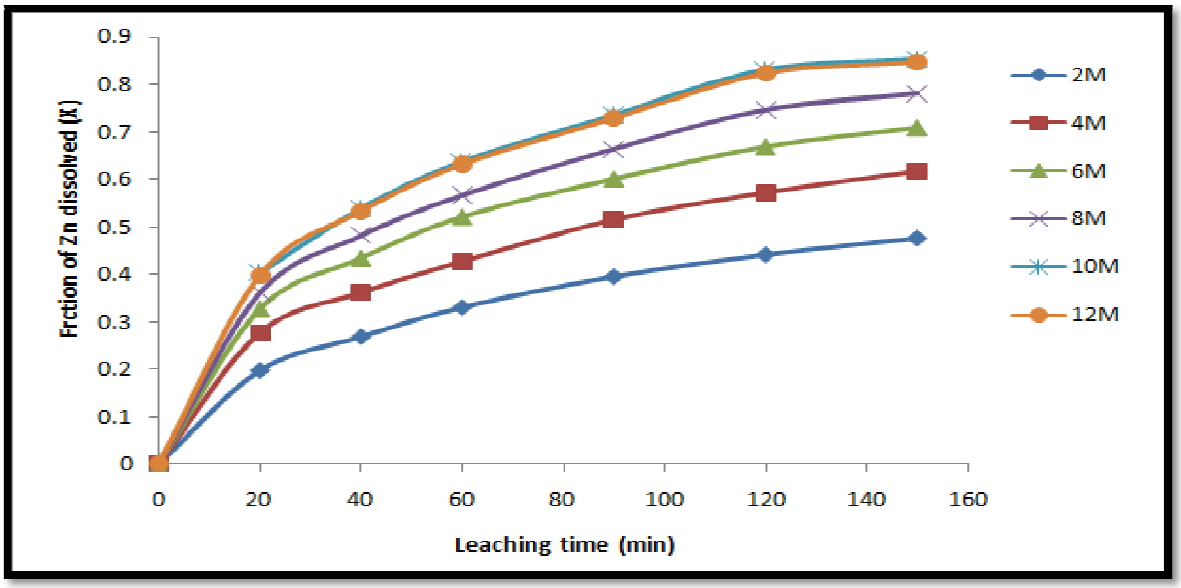

Figure 4: Effect of HNO_3 Concentration on Sphalerite Dissolution at Various LeachingTime Experimental Conditions: Particle Size = 75 µm; Solid/Liquid Ratio = 20g/L; Temperature = 333 K; Stirring Speed = 450 Rpm

3.2.2. Effect of Stirring Rate on Sphalerite Dissolution

The results on the effect of stirring rate on sphalerite dissolution in 10M HNO_3 over the range of 90-720 rpm at 363K is presented in Figure 5.

Figure 5 shows that the amount of sphalerite dissolved is dependent on the stirring speed over the range 90-540 rpm. Above 540 rpm, the stirring speed no longer has any observable effect on the solid dissolution. Hence dissolution reached a steady rate at 540 rpm, and a stirring speed of 540 rpm was retained for further experiments. Increase in stirring speed causes a decrease in the thickness of the film layer, therefore, causing an increase in the dissolution rate (Ajemba and Onukwuli, 2012).

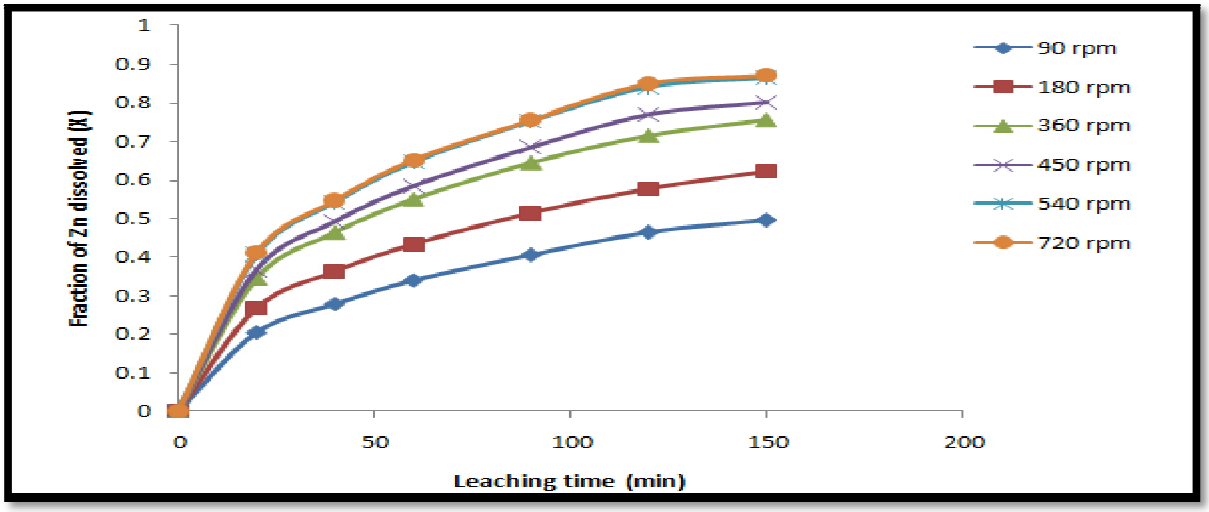

Figure 5: Effect of Stirring Rate on Sphalerite Dissolution at Various Leaching Time
Experimental Conditions: Particle Size = 75 µm; Solid/Liquid Ratio = 20g/L; Temperature = 363 K; HNO_3 Concentration = 10M

3.2.3. Effect Of Temperature On Sphalerite Dissolution

The effect of temperature on sphalerite dissolution has been investigated over the temperature range 303-363 K in 10 M HNO_3 solution at a stirring rate of 540 rpm using 75 µm particle diameter and solid/liquid ratio of 20 g/L. These results are presented in Figure 6.

As seen in Figure 6, sphalerite dissolution increases with increase in leaching time and with increasing temperature. This is as a result of high kinetic energy available for the reacting molecules (Ajemba and Onukwuli, 2012). For instance, at 363 K, the amount of sphalerite dissolved within 150 min was 86.5%.

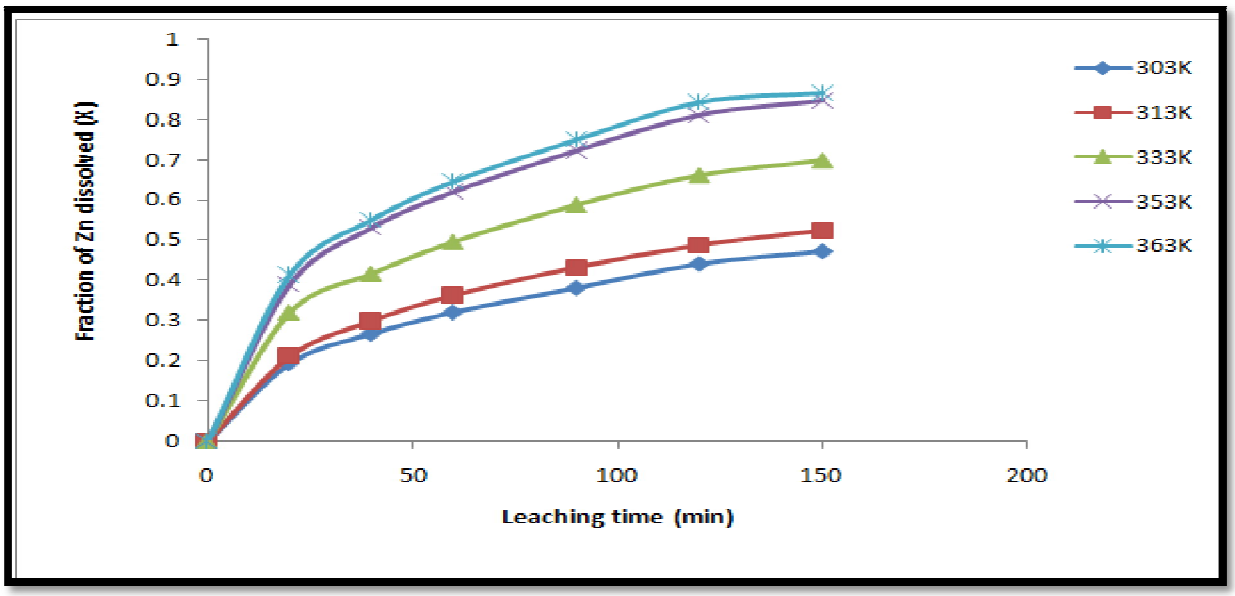

Figure 6: Fraction of Sphalerite Dissolved Vs. Leaching Time at Different Temperatures
Experimental Conditions: Particle Size = 75 µm; Solid/Liquid Ratio = 20g/L; Stirring Rate = 540 Rpm; HNO_3 Concentration = 10M

3.2.4. Effect Of Solid/Liquid Ratio On Sphalerite Dissolution

The results on the effect of solid/liquid ratio on sphalerite dissolution in 10 M HNO_3 were investigated in the range 0.02 to 0.045 g/ml at a temperature of 363 K .

Figure7 shows the effect of solid/liquid ratio on sphalerite dissolution in 10 M HNO_3. Decreasing the solid/liquid ratio is accompanied with increase in the equilibrium percentage of the ore dissolved. For instance, by varying the solid/liquid ratio from 0.045 to 0.02 g/ml, the percentage of sphalerite dissolved increased from 49.8% to 86.2% at 363 K. This could be attributed to the decrease in the fluid reactant per unit weight of the solid (Ajemba and Onukwuli, 2012). Accordingly, an optimum solid/liquid ratio 0.02 g/ml has been retained for subsequent studies.

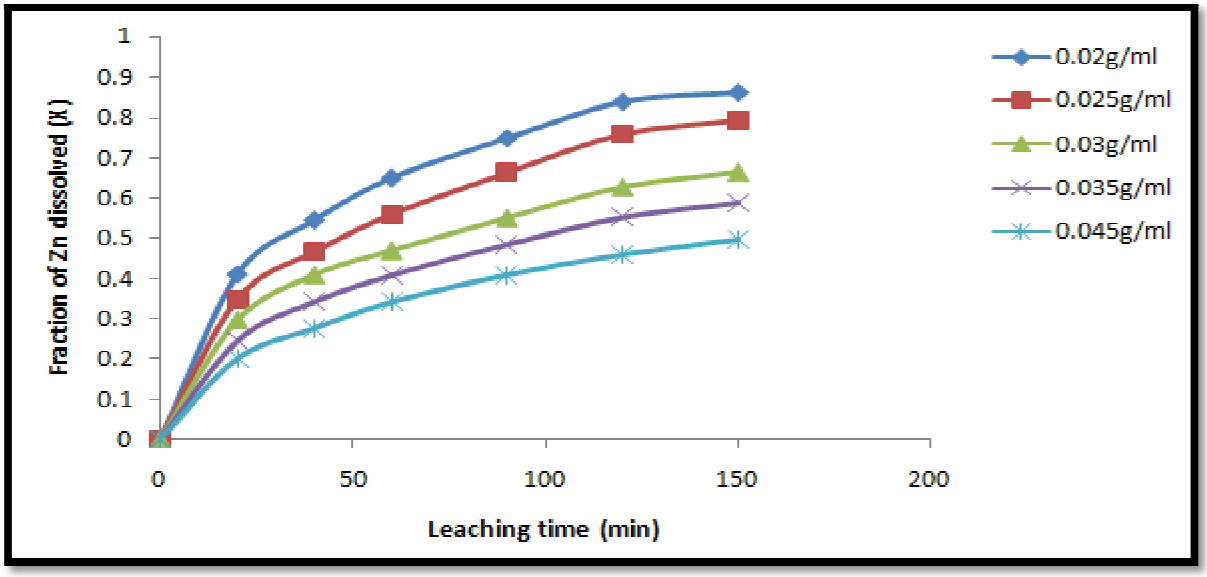

Figure 7: Effect of Solid/Liquid Ratio on Sphalerite Dissolution
Experimental Conditions: HNO_3 Concentration = 10 M; Particle Diameter = 75 µm; Stirring Rate = 540 Rpm; Temperature = 363 K

3.2.5. Effect of Particle Size on Sphalerite Dissolution

The influence of particle diameter on sphalerite dissolution in HNO_3 was investigated for five different sized fractions. The results are summarized in Figure 8.

The results from Figure 8 showed that the smaller the sphalerite particle size, the faster was the sphalerite dissolution. This is attributed to larger specific surface area provided by the smaller particles for contact with the acid molecules (Ajemba and Onukwuli, 2012). This observation was also supported by Aydogan et al. (2007a) and Dutrizac and MacDonald (1977).

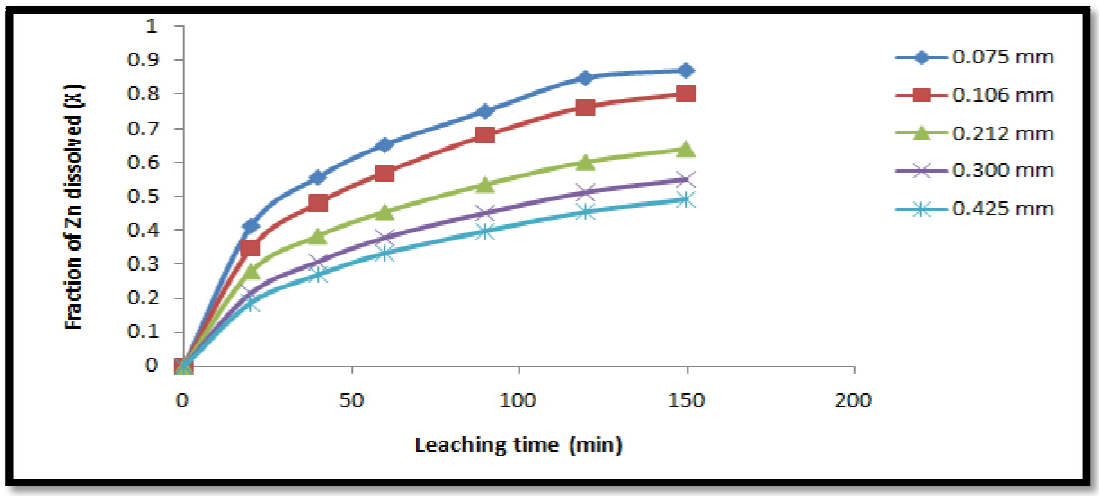

Figure 8: Effect of Particle Diameter on Sphalerite Dissolution
Experimental Conditions: HNO_3 Concentration = 10 M; Solid/Liquid Ratio = 20 G/L; Stirring Rate = 540 Rpm; Temperature = 363 K

3.3. Dissolution Kinetic Models

The dissolution rates were analyzed with the shrinking core models which state that the leaching process is controlled by:

- The rate of the surface chemical reaction (Levenspiel, 1972);
- By the diffusion of reactant through the solution boundary layer, or through a solid product layer; or
- By mixed controlled process (Chemically and diffusion-controlled reactions).

For this study, three shrinking core models were tested for better understanding of the dissolution of sphalerite in HNO_3 media. The kinetic models as previously utilized by some authors such as Aydogan et al. (2007a,b), Baba and Adekola (2010), Habashi (2005), Khalique et al. (2005), Leao (2007) and Merwe (2003) include:

$1 - (1 - X)^{1/3} = \frac{bk_s C_A}{\rho_s r_o} t = k_2 t$ (2)

$1 + 2(1 - X) - 3(1 - X)^{2/3} = \frac{6bD_e C_A}{\rho_s r_o^2} t = k_3 t$ (3)

$1 - (1 - X)^{1/3} + (y/6)[(1 - X)^{1/3} + 1 - 2(1 - X)^{2/3}] = k_4 t$ (4)

where X is the fraction of sphalerite dissolved at time t, b the stoichiometric coefficient of the reagent in the leaching reaction, k_s the kinetic constant, C_A the concentration of nitric acid (HNO_3), ρ_s the density of the solid, r_o the initial radius of the solid, and k_2 the rate constant from Equation (2). D_ϵ is the effective diffusion coefficient, k_3 and k_4 are the rate constants for Equations (3) and (4) respectively, y is taken to be 1 for heterogeneous systems.

Equation (2) is applicable to a chemical reaction controlled process at the interface; Equation (3) is a diffusion-controlled process through the product layer and Equation (4) is a mixed controlled process (a combination of surface reaction and diffusion). Of all the three models tested, all the studied data were found only to fit the relation in Equation (3) with a perfect correlation of about 0.99. The analysis of the plots of other kinetic curves, however, gave lower correlation coefficients. Hence, the linearization of Figures 4 – 8 was made. To this end, the relation:

$1 + 2(1 - X) - 3(1 - X)^{2/3} = k_1 t$, gave an average correlation coefficient of 0.994 and this is shown in Figure 9.

From Figure 9, the experimental rate constant k_1, was calculated from the slope of the straight line at various HNO_3 concentrations and the plots of In k_1 versus In [HNO_3] are shown in Figure 10.

From Figure 10, the slope of the resulting plot gave 0.91. This shows that the order of reaction with respect to H^+ ion concentration is 0.91 with correlation coefficient of 0.990.

Similarly, the apparent rate constant k_5 was calculated from the slope of the straight line at various stirring rates (w) as shown in Figure 11 and the plots of In k_5 versus In w are shown in Figure 12.

Furthermore, the data in Figure 6 at different temperatures were linearized by Equation (3). This is shown in Figure 13. The data in Figures 7 and 8 were also linearized by means of Equation (3) as shown in Figures 15 and 16 respectively.

From Figure 13, the apparent rate constants, k_3 and other tested constants, k_2 and k_4 were calculated from the slopes of the straight lines. The values of these rate constants with their equivalent correlation coefficients are summarized in Table 3.

Temperature (K)	Apparent rate constants (10^{-3} min^{-1})			Correlation coefficient, R^2		
	K_2	K_3	K_4	K_2	K_3	K_4
303	1.5	0.66	2.16	0.803	0.998	0.783
313	1.70	0.84	2.45	0.806	0.998	0.785
333	2.57	1.77	3.61	0.809	0.996	0.776
353	3.56	3.08	4.87	0.857	0.996	0.815
363	3.78	3.40	5.14	0.853	0.991	0.808

Table 3: The Values of Rate Constants K_2, K_3 and K_4 with Their Correlation Coefficients For Sphalerite Dissolution at Different Temperatures by 10M HNO_3

By using the rate constants derived from the slopes in Figure 13, the Arrhenius diagram in Figure 14 was plotted from which the activation energy of 26.42KJ/mol was calculated.

3.3.1. Evaluation of Activation Energy of Sphalerite Dissolution in HNO_3

Some of the reported activation energies, Ea, of sphalerite dissolution are presented in Table 4. From Table 4, it was observed that Abakaliki sphalerite (Nigeria) exhibited the least activation energy. Thus, Abakaliki sphalerite can be said to be kinetically much favorable to leaching by HNO_3 compared to other sphalerite types.

A value of 23.1s^{-1} was subsequently obtained for the Arrhenius constant and with a corresponding correlation coefficient of 0.989.

The Arrhenius constant is proportional to the pre-exponential factor A or frequency factor. This is otherwise referred to as the frequency of collision between species (collision number) which vary from one system to another (Mortimer and Taylor, 2002).

According to Olanipekun (1999), the rate controlling mechanism of heterogeneous dissolution process is often predicted from the plots of the kinetic equations, rather than the activation energy. Therefore, in order to determine the rate determining step for the present study, the kinetic curves in Figure 7 were also linearized by means of Equation (3). The values of the rate constants, k, were plotted against the reciprocal of the particle radii ($1/r_o$), yielding a linear relationship with a correlation coefficient of 0.995 (Figure 19). It is interesting to note that the plot of the rate constants as a function of the square of particle radii $(1/r_o)^2$ did not give a linear relationship. This indicates that the surface chemical reaction was the rate controlling step during the dissolution (Antonijevic et al., 1997).

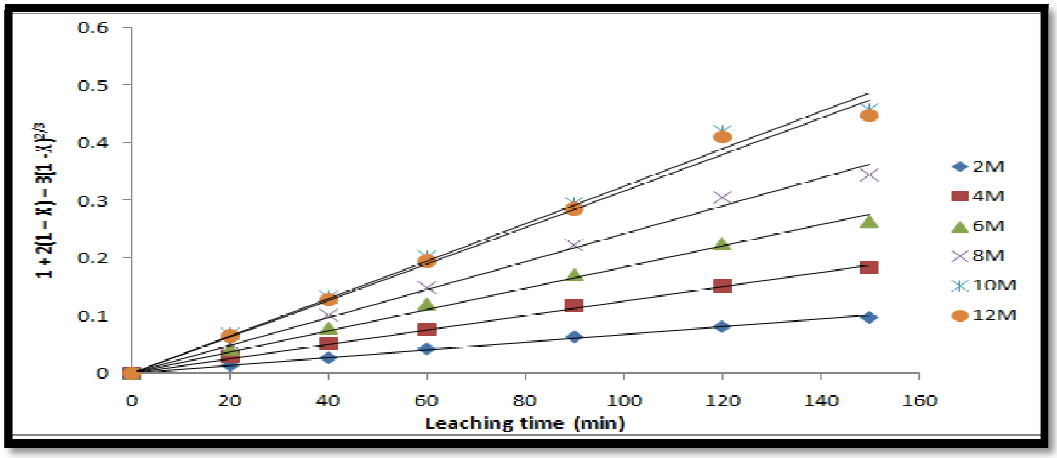

Figure 9: Plot of 1 + 2(1 – X) – 3(1 -X) $^{2/3}$ = Kt vs. Leaching Time at Various HNO_3 Concentrations for Data Presented in Figure 4

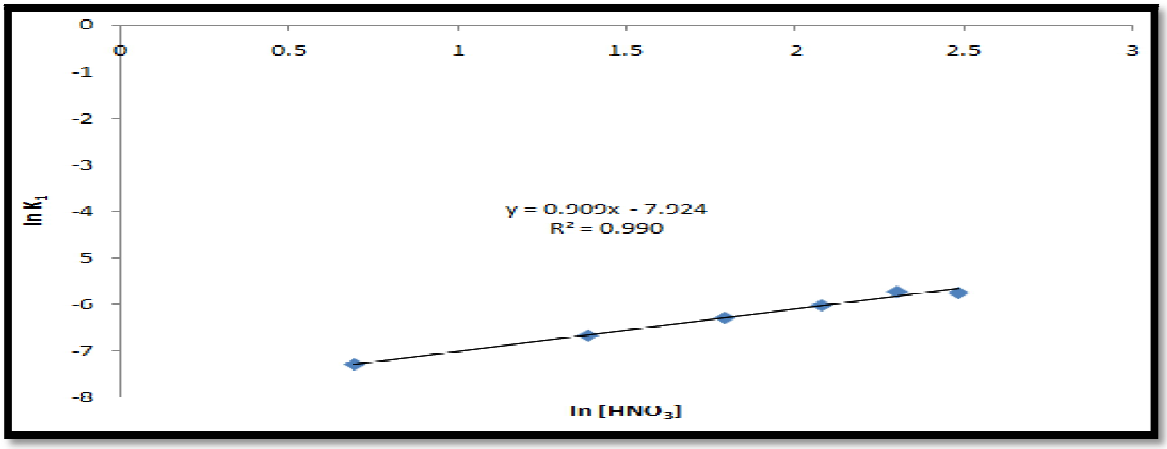

Figure 10: Plot of In k_1 Vs. In $[HNO_3]$, For Determining Order of Acid Concentration

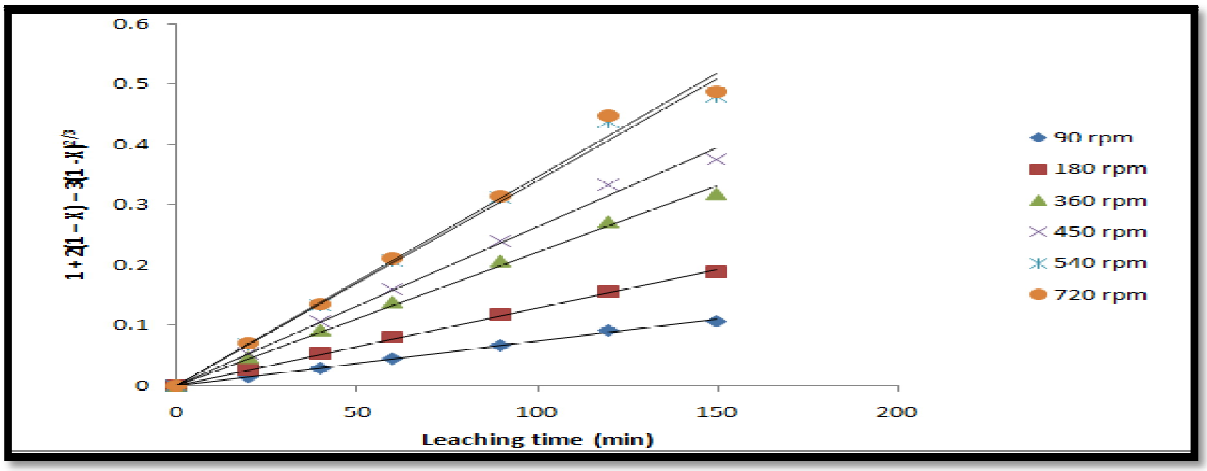

Figure 11: Plot of 1 + 2(1 – X) – 3(1 -X) $^{2/3}$ = K T vs. Leaching Time at Various Stirring Rates for Data Presented in Figure 5

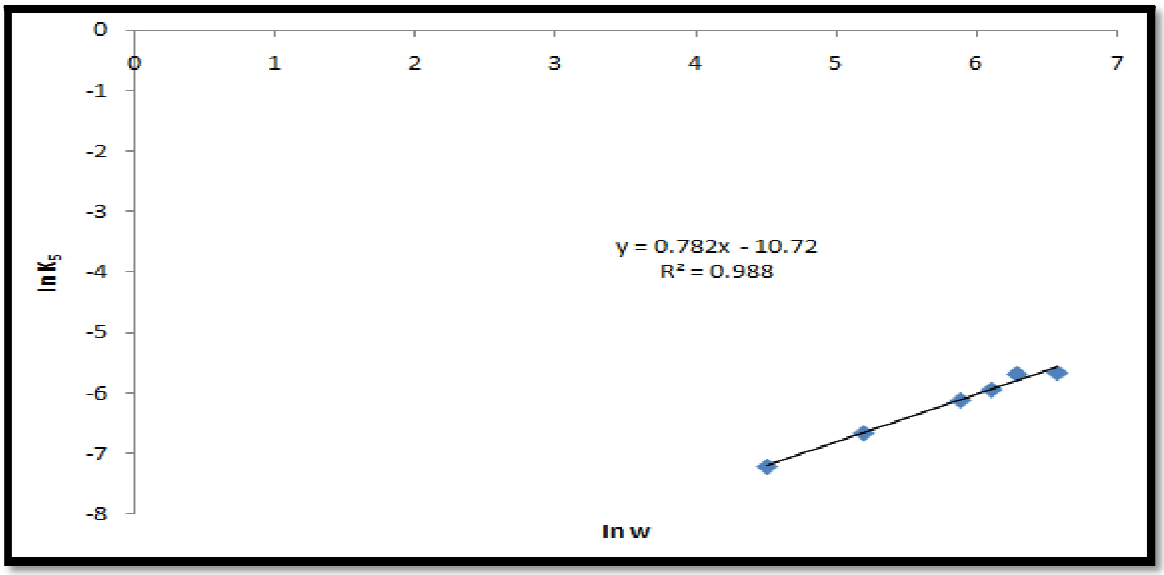

Figure 12: Plot of in k_5 Vs. In W, For Determining Order of Stirring Rate

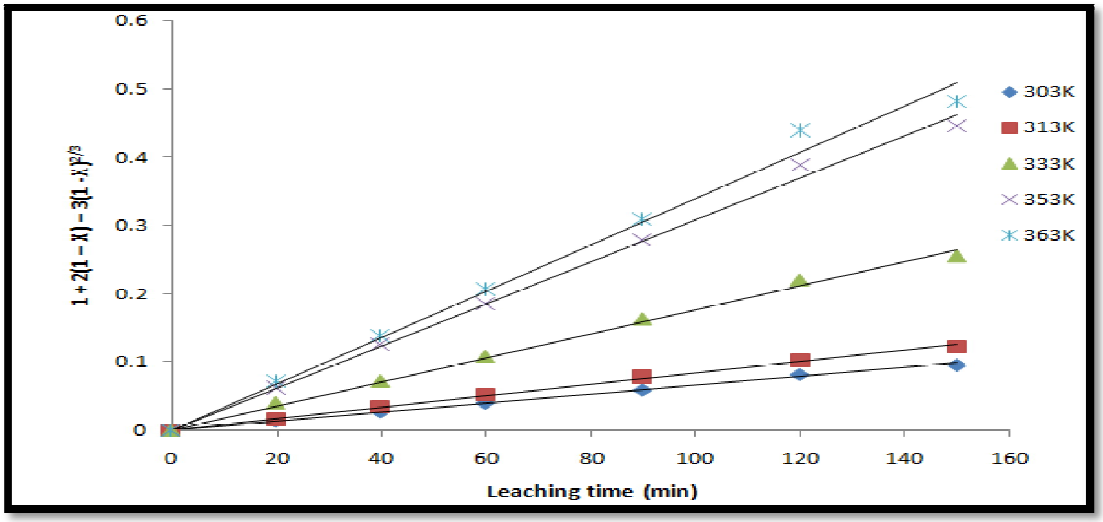

Figure 13: Plot of 1 + 2(1 – X) – 3(1 -X) $^{2/3}$ = K T vs. Leaching Time at Various Temperatures for Data Presented in Figure 6

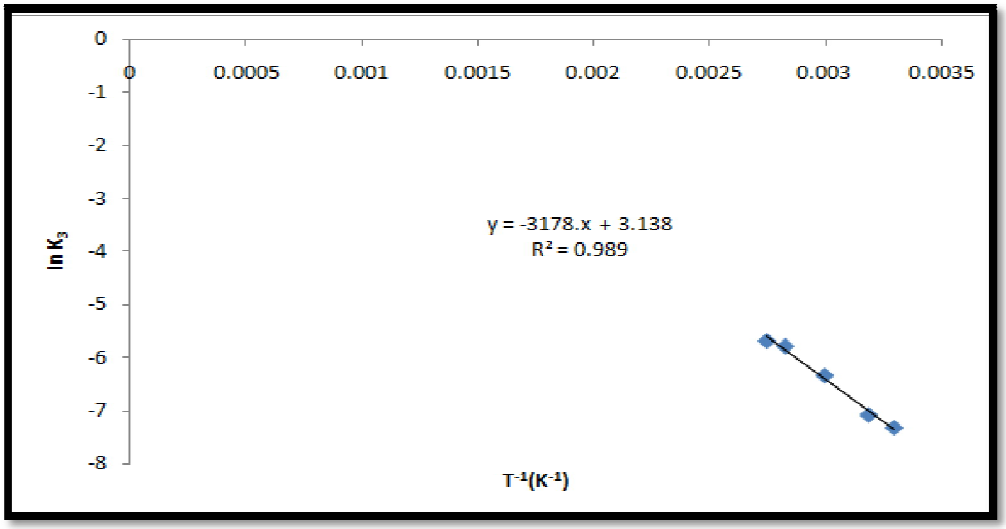

Figure 14: Arrhenius Plot of Reaction Rate against Reciprocal of Temperature

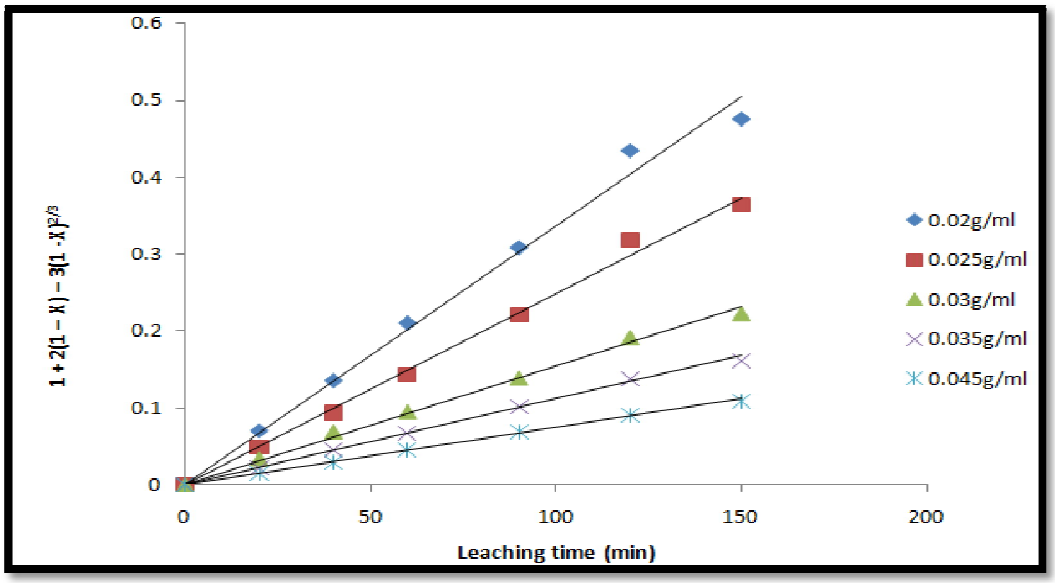

Figure 15: Plot of 1 + 2(1 – X) – 3(1 -X) $^{2/3}$ = K T vs. Leaching Time at Various Solid/Liquid Ratios for Data Presented in Figure 7

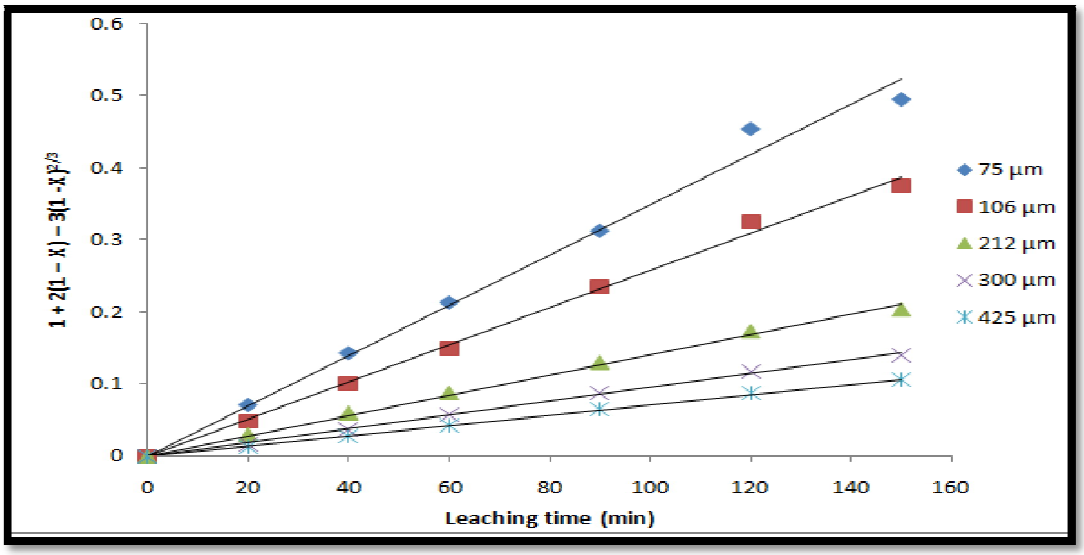

Figure 16: Plot of 1 + 2(1 – X) – 3(1 -X) $^{2/3}$ = K T vs. Leaching Time at Various Particles Diameters for Data Presented in Figure 8

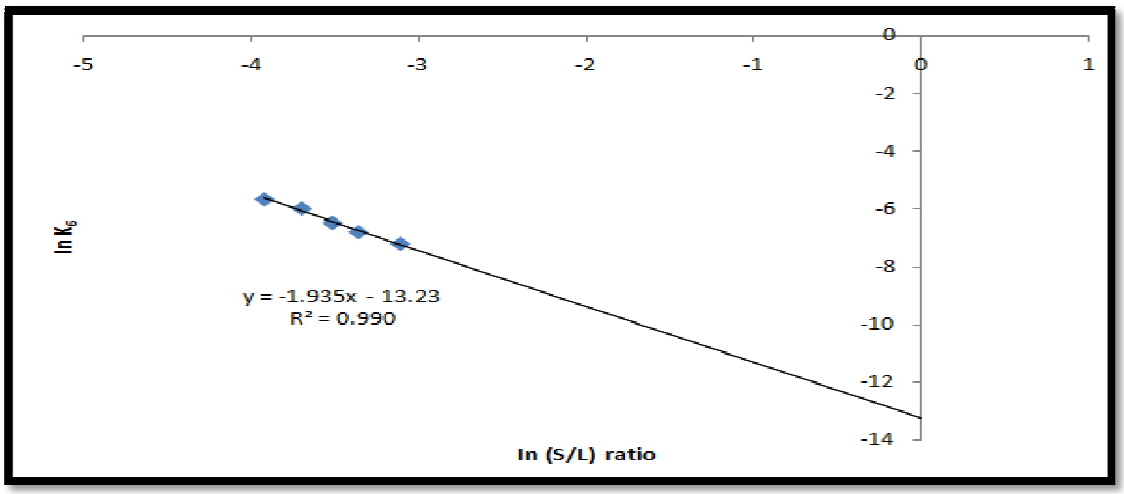

Figure 17: Plot Of In k_6 Vs. In (S/L), for Determining Order of Solid/Liquid Ratio

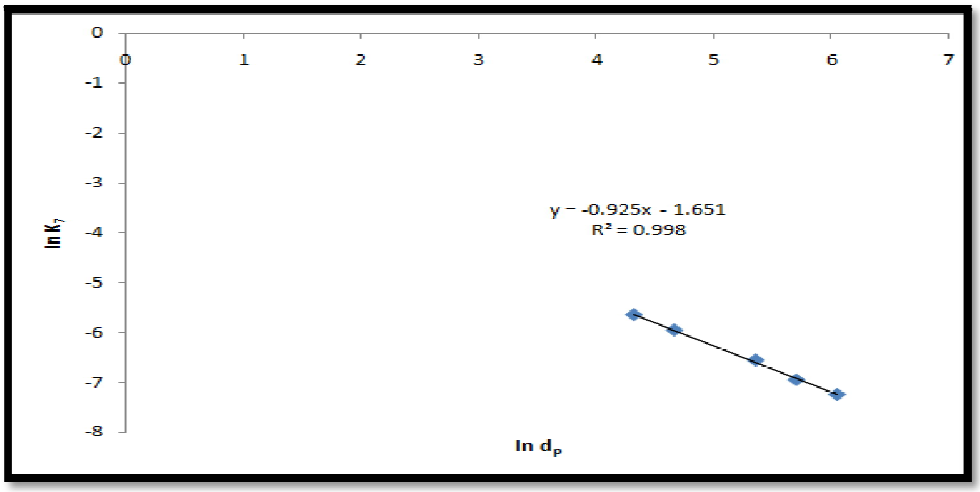

Figure 18: Plot Of In k_7 Vs. Ind_p, for Determining Order of Initial Particle Diameter

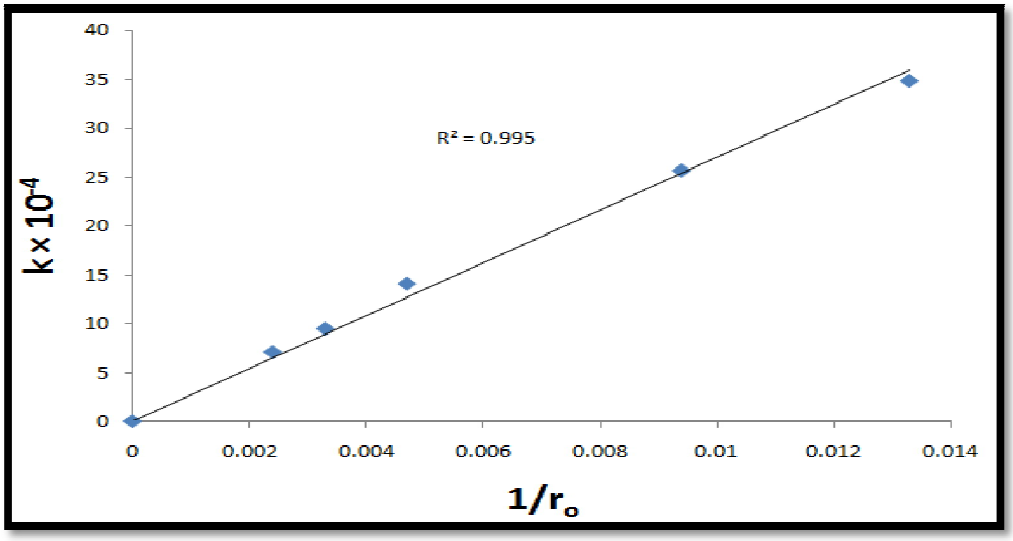

Figure 19: Dependence of Rate Constant, K, on $1/R_o$

Origin of sphalerite	Leachant	Ea (KJ/mol)	References
Bhubaneswar, India	4 M HCl H_2O_2	46.5	Madhuchhanda et al.(2000)
Bhubaneswar, India	4 M HCl/1 M MnO_2	56.7	Madhuchhanda et al. (2000)
Japan	12 M HCl	84.0	Majima et al. (1981)
Sivas, Turkey	0.25 M $FeCl_3$/0.1 M HCl	45.3	Aydogan et al. (2005)
Pittsburgh, China	0.2 M $FeCl_3$/0.1 M HCl	58.4	Zuo-mei et al. (1984)
Abakaliki, Nigeria	4 M HCl	39.1	Baba and Adekola (2010)
Abakaliki, Nigeria	10 M HNO_3	26.4	This study

Table 4: Some Reported Activation Energies for Sphalerite Leaching by Different Leaching Systems

3.3.2. Dissolution Model

From the effects of the solid/liquid ratio (Figure 17) and particle diameters (Figure 18) on sphalerite dissolution in 10M HNO_3 solution, the apparent rate constants, k_6 and k_7 were evaluated, respectively.

The solid/liquid ratio and initial particle size (d_p) were found to be inversely proportional to 1.94 power $(S/L)^{-1.94}$ and 0.93 power ($d_p^{-0.93}$), respectively. Hence, the proposed model equation for sphalerite dissolution by 10M HNO_3 solution at 363K is consistent with the following relation:

$$1 + 2(1-X) - 3(1-X)^{2/3} = k_o C_{HNO_3}^{0.91} (d_p)^{-0.93} \left(\rho \frac{S}{L}\right)^{-1.94} (w)^{0.78} e^{(-26422/RT)}\ t$$

where ρ is the ore density (Baba and Adekola, 2011). k_o is a reaction constant, which can be determined from the fraction of sphalerite ore dissolved, X at a given time, t. The parameter, X is determined experimentally. For instance, at 363K, the value of

X = 0.866 (86.6% dissolution); k_o is calculated to be 5.23×10^7. The value of k_o , however, is found to vary depending on the leaching systems/conditions (Aydogan et al., 2007; Fuerstenau et al., 1986).

3.4. Characterization of the Residual Product

3.4.1. SEM Analysis of Sphalerite Leached with 10M HNO_3

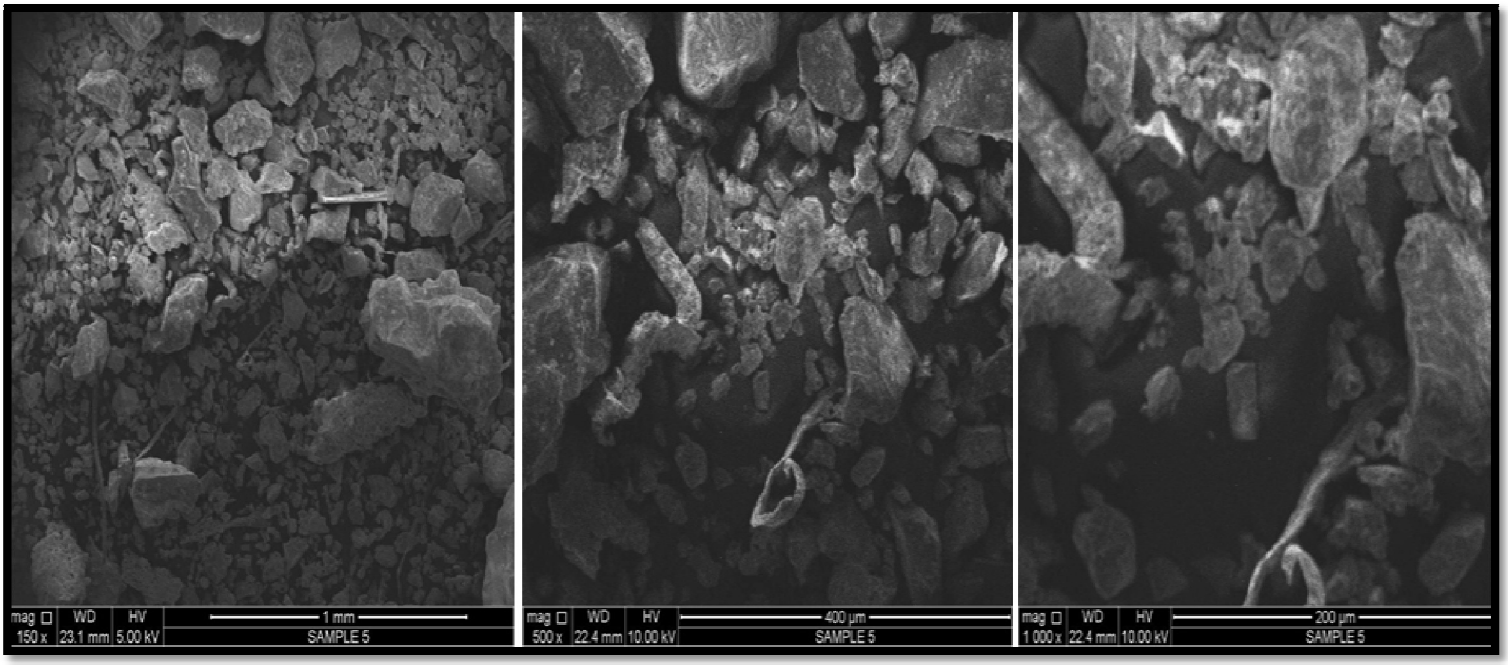

Figure 20: Figure 20 SEM Image of Sphalerite Leached with 10M HNO_3 with Magnifications of 150× (A), 500× (B), 1000× (C) Respectively

The morphology of sphalerite after leaching with 10M HNO_3 was examined with by scanning electron micrograph (SEM) and obtained with magnifications of 150×, 500× and 1000× respectively as shown in Figure 20. The average cell diameter ranges from 38 to 116µm while the average cell density ranges from 0.0688 to 0.142 cell/mm. The micrographs of the leaching residues show a progressive increase in the roughness of the solid and also an increase in the amount of elemental sulphur covering the particle surfaces (Souza et al., 2007).The particles have irregular shapes and form microscopic flakes and may be poorly crystalline due to attack by the lixiviant.

3.4.2. XRD Analysis Of Sphalerite Leached With 10 M HNO_3

The analysis of sphalerite leached with 10M HNO_3 at 363K by X-ray diffraction gives a description of the mineral phases present in the residue. Table 5 present the results of the X-ray diffractogram of the residue. The result showed three major peaks at 3.85, 3.22, and 3.45 Å, respectively as shown in Figure 21. The XRD data revealed the presence of sulphur, quartz and sylvite. The result agrees with the SEM results of the residue. It is important to note the absence of zinc in the residual product.

2θ	d-Value (Å)	Compound	Intensity (%)	JCPDS file No
21.89	4.06	Sulphur (S_{128})	15.65	96-900-8578
23.08	3.85	Sulphur (S_{128})	100.00	96-900-8578
25.85	3.45	Sulphur (S_{128})	48.27	96-900-8578
26.71	3.34	Sulphur (S_{128}) Quartz (Si_6O_6)	41.64	96-900-8578 96-900-0776
27.73	3.22	Sulphur (S_{128}) Sylvite (K_4Cl_4)	70.65	96-900-8578 96-900-3134
28.65	3.11	Sulphur (S_{128})	31.42	96-900-8578
31.39	3.09	Sulphur (S_{128})	24.52	96-900-8578
33.35	2.85	Sulphur (S_{128})	27.12	96-900-8578
42.46	2.13	Quartz (Si_6O_6)	37.60	96-900-0776

Table 5: The X-Ray Diffraction Data of the Sphalerite Ore Leached with 10M HNO_3 Showing the Angle 2θ and D-Values of the Compounds Identified, with Their Relative Intensity (%)

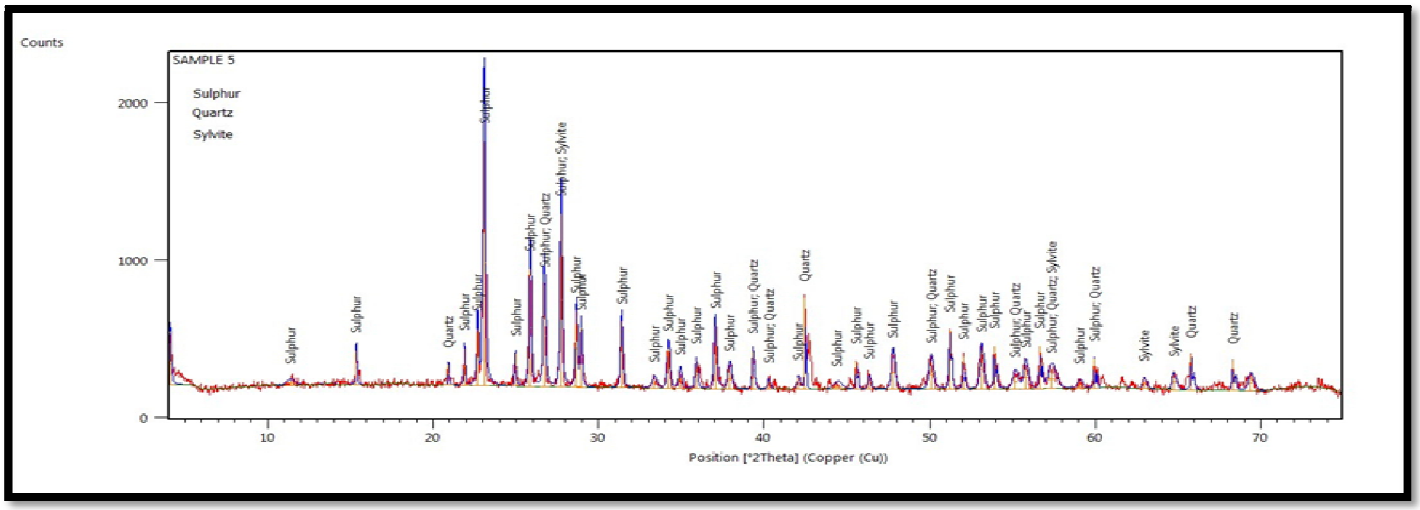

Figure 21: X-Ray Diffraction Pattern of the Post-Leached Residue of Sphalerite After Leaching For 150 Minutes at 363K with 10M HNO_3

4. Conclusions

On the basis of the results of the characterization and dissolution studies undertaken in this study, the following conclusions can be drawn: i. The X-ray fluorescence data showed that the sphalerite mineral used in the study exist mainly as ZnS. Zinc (Zn) was detected as the major metal for sphalerite with metals such as Na, Ca, Fe, Al and Mg occurring as minor elements. The XRD analysis also confirmed the originality of the sphalerite ore as it revealed the presence sphalerite as the dominant mineral and cerium germanium sulphide as an associated mineral. The Fourier transform infrared (FTIR) analysis also supported the XRF and XRD analysis by revealing the presence of sulphur. The scanning electron micrograph (SEM) analysis revealed a high level of crystallinity of the ore. ii. The leaching investigation clearly showed that sphalerite dissolution in nitric acid (HNO_3) increased with increasing concentration of nitric acid, temperature and stirring rate, and decreased with increasing particle diameter and solid/liquid ratio. In 10M HNO_3 at a temperature of 363K using 75µm particle diameter with solid/liquid ratio of 20g/L and stirring speed of 540 rpm, about 86.6% of sphalerite was dissolved in 150 minutes. The values of activation energy, order of reaction and Arrhenius constant calculated at the conditions above for sphalerite were 26.42 KJ/mol, 0.91 and 23.06 s^{-1} respectively. iii. The results of the dissolution studies indicated that the data fitted the shrinking core model for the diffusion-controlled mechanism, with surface chemical reaction as the rate controlling step. This is consistent with the following relation:

$1 + 2(1 - X) - 3(1 - X)^{2/3} = k_0 C_{HNO_3}^{0.91} (d_p)^{-0.93} (\rho \frac{S}{L})^{-1.94} (w)^{0.78} e^{(-26422/RT)}$ t; where k_0 is the reaction constant, which can be determined experimentally.

iv. The post-leaching residue was found to be constituted of sulphur, quartz and sylvite.

5. References

i. Adebayo, A. O., Ipinmoroti, K. O., Ajayi, O. O. (2006). Leaching of Sphalerite with Hydrogen Peroxide and Nitric Acid Solutions. Journal of Minerals & Materials Characterization & Engineering, Vol. 5, No. 2, pp. 167 – 177.

ii. Ajemba, R. O., Onukwuli, O. D. (2012). Determination of the optimum dissolution conditions of Ukpor clay in hydrochloric acid using Response Surface Methodology. International Journal of Engineering Research & Applications, vol. 2, Issue 5, pp. 732-742.

iii. Al – Harahsheh, M., Kingman, S. (2007). The influence of microwaves on the leaching of sphalerite in ferric chloride. Chemical Engineering and Processing 46, 883 – 888.

iv. Antonijevic, M. M., Dimitrijevic, M., Jankovic, Z. (1997). Leaching of pyrite with hydrogen peroxide in sulphuric acid. Hydrometallurgy 46, 71 – 83.

v. Aydogan, S., Aras, A., Cambazoglu, M. (2005). Dissolution kinetics of sphalerite in acidic ferric chloride Leaching. Chem. Eng. J., 114, 67-72.

vi. Aydogan, S., Erdemoglu, M., Ucar, G., Aras, A. (2007a). Kinetics of galena dissolution in nitric acid solutions with hydrogen peroxide. Hydrometallurgy, 88, 52-57.

vii. Aydogan, S., Erdemoglu, M., Ucar, G., Aras, A. (2007b). Dissolution kinetics of galena in acetic acid solutions with hydrogen peroxide. Hydrometallurgy 89,189-195.

viii. Baba, A. A., Adekola, F. A. (2010). Hydrometallurgical Processing of a Nigerian Sphalerite in Hydrochloric Acid: Characterization and dissolution kinetics, Hydrometallurgy, 101: 69 – 75.

ix. Baba, A. A., Adekola, F. A. (2011). Comparative analysis of the dissolution kinetics of galena in binary solutions of $HCl/FeCl_3$ and HCl/H_2O_2. International Journal of Minerals, Metallurgy and Materials, Volume 18, Number 1.

x. David R. L. (2006). Handbook of chemistry and physics, 87th ed., Boca Raton, Florida: CRC Press, Taylor & Francis Group.

xi. Dutrizac, J. E., MacDonald, R. J. C. (1977). CIM Annual Volume, 186 – 194.

xii. Emsley, J. (2001). "Zinc" Nature's building blocks: An A-Z guide to the elements. Oxford, England, UK: Oxford, England, UK: Oxford University Press. pp. 499-505.

xiii. Frenzel, M., Ketris, M. P., Seifert, T., Gutzmer, J. (2016). On the current and future availability of gallium. Resources Policy. 47: 38 – 50.

xiv. Frenzel, M., Ketris, M. P., Gutzmer, J. (2016). On the geological availability of germanium. Mineralium Deposita. 49(4): 471 – 486. DOI: 10.1007/s00126-013-0506-z

xv. Frenzel, M., Mikolajczak, C., Reuter, M. A., Gutzmer J. (2017). Quantifying the relative availability of high-tech by – product metals - The cases of gallium, germanium and indium. Resources Policy. 52: 327- 335. DOI:10.1016/j.resourpol.2017.04.008.

xvi. Feursternau, M. C., Nebo, C. O., Elango, B. V., Han, K. H. (1986). The kinetics of leaching galena with ferric nitrate, Metal Trans., B, 18B, 25 – 30.

xvii. Goktepe, F.(2002). Effect of pH on pulp potential and sulphide mineral flotation, Turk. J. Eng. Sci., 26, 309 – 318.

xviii. Habashi, F. (2005). Hydrometallurgy of lead. Metallurgia 59 (3), 114 -118.

xix. Harvey, T. J., Yen, W. T. (1998). The influence of chalcopyrite, galena and pyrite on the selective extraction of zinc from base metal sulphide concentrates. Minerals Engineering, 11(1), 1-21.

xx. Heiserman, D. L. (1992). Element 30: Zinc. Exploring chemical elements and their compounds. New York: TAB Books.

xxi. Hutchison, C. S.(1974). Laboratory Handbook of Petrography Techniques, first ed. John Wiley and Sons Inc., New York, pp. 1-14.

xxii. Khalique, A., Akram, A., Ahmed, A. S., Hamid, N. (2005). Effect of sodium chloride on dissolution of galena in aqueous acid solution. Pak. J. Sci. Ind. Res. 48 (4), 236 – 239.

xxiii. Konstantinou, I. K., Albanis, T. A. (2004). Worldwide occurrence and effects of antifouling paint booster biocides in the aquatic environment: a review. Environment International 30 (2): 235-248. DOI: 10.1016/S0106-4120(03)00176-4.

xxiv. Leao, V. A., Souza, A. D., Pina, P. S., Silva, C. A., Siqueira, P. F. (2007). The leaching kinetics of a zinc sulphide concentrate in acid ferric sulphate, Hydrometallurgy, 89; 72 – 81.

xxv. Levenspiel, O. (1972). Chemical Reaction Engineering, 2nd edition, John Wiley & Sons. New York.

xxvi. Madhuchhanda, M., Devi, N. B., Rao, K. S., Rath, P. C., Paramguru, R. K. (2000). Oxidation of sphalerite in hydrochloric acid medium in the presence of manganese dioxide., Inst. Min. Metall. ,109, CISO-CISS.

xxvii. Majima, H., Awakura, Y., Misaki, N. (1981). A Kinetic Study on Non-Oxidative Dissolution of Sphalerite in Aqueous Hydrochloric Acid Solutions. Metall. Trans. B 12B, 645 – 649.

xxviii. Merwe, W. (2003). Dissolution of sphalerite minerals from Rosh Pinah Tailings, Magister Scientiae, Faculty of Natural and Agric. Sciences, University of Pretoria, p. 106.

xxix. Mortimer, M., Taylor, P. (2002). The molecular world chemical kinetics and mechanis, Bath Press Colour books, Glasgow, pp. 19-33.

xxx. Olanipekun, E. O., Oderinde, R. A. (1999). Hydrochloric acid leaching of sphalerite in the presence of anoxidizing agent, Park. J. Sci. Ind. Res. 42(4), 204 – 208.

xxxi. Paschotta, R. (2008). Encyclopedia of Laser Physics and Technology. Wiley-VCH. P.798. ISBN 3-527-40828-2.

xxxii. Peng, P., Xie, H., Lu, L. (2005). Enhanced leaching of sphalerite concentrate in H_2SO_4-HNO_3 solutions andextraction of sulphur with tetrachloroethylene. Hydrometallurgy, 80, 265.

xxxiii. Sassi, A. B., Sassi, S. (1999). Cadmium associated with phosphate deposits in southern Tunisia, J. Afr. Earth Sci. 29(3), 501 -513.

xxxiv. Sokic, M., Markovic, B., Matkovic, V., Zivkovic, D., Strbac, N., Stojanovic, J. (2012). Kinetics and mecha-nism of sphalerite leaching by Sodium Nitrate in Sulphuric acid Solution, Journal of Mining and Metallurgy, 48(2), 185 – 195.

xxxv. Sthay, C., Ramaswamy, S. (2002). Influence of mineral impurities on the properties of kaolin and its thermally treated products. Appl. Clay Sci. 21, 133 – 142.

xxxvi. Ucar, G. (2009). Kinetics of sphalerite dissolution by sodium chlorate in hydrochloric acid, Hydrometallurgy 95, 39 – 43.

xxxvii. Warren, G. W., kim, S., Henein, H.(1986). The effect of chloride ion on the ferric chloride leaching of galena concentrate, Metall. Mater. Trans. B., 18, p. 59.

xxxviii. Zhang, X. G. (1996). Corrosion and Electrochemistry of Zinc. Springer. P. 93. ISBN 0-306-45334-7

xxxix. Zuo-mei, J., Warren, G. W., Henein, H. (1984). Reaction kinetics of ferric chloride leaching of sphalerite: an experimental study. Metall. Trans. B. 15B, 5 -12.